Renal crystal deposits and histopathology in patients with cystine stones

AP Evan[1], FL Coe[2], JE Lingeman[3], Y Shao[4], BR Matlaga[3], SC Kim[3], SB Bledsoe[1], AJ Sommer[5], M Grynpas[6], CL Phillips[7] and EM Worcester[2]

[1]Department of Anatomy and Cell Biology, Indiana University School of Medicine, Indianapolis, Indiana, USA; [2]Nephrology Section, University of Chicago, Chicago, Illinois, USA; [3]International Kidney Stone Institute, Methodist Clarian Hospital, Indianapolis, Indiana, USA; [4]Department of Histology, Jinzhou Medical College, Jinzhou, Liaoning, People's Republic of China; [5]Department of Chemistry and Biochemistry, Miami University, Oxford, Ohio, USA; [6]Samuel Lunenfeld Research Institute, Mount Sinai Hospital, Toronto, Canada and [7]Department of Pathology, Indiana University School of Medicine, Indianapolis, Indiana, USA

We have biopsied the papillae of patients who have cystine stones asking if this stone type is associated with specific tissue changes. We studied seven cystine stone formers (SF) treated with percutaneous nephrolithotomy using digital video imaging of renal papillae for mapping and obtained papillary biopsies. Biopsies were analyzed by routine light and electron microscopy, infrared spectroscopy, electron diffraction, and micro-CT. Many ducts of Bellini (BD) had an enlarged ostium, and all such were plugged with cystine crystals, and had injured or absent lining cells with a surrounding interstitium that was inflamed to fibrotic. Crystal plugs often projected into the urinary space. Many inner medullary collecting ducts (IMCD) were dilated with or without crystal plugging. Apatite crystals were identified in the lumens of loops of Henle and IMCD. Abundance of interstitial Randall's plaque was equivalent in amount to that of non-SF. In the cortex, glomerular obsolescence and interstitial fibrosis exceeded normal. Cystine crystallizes in BD with the probable result of cell injury, interstitial reaction, nephron obstruction, and with the potential of inducing cortical change and loss of IMCD tubular fluid pH regulation, resulting in apatite formation. The pattern of IMCD dilation, and loss of medullary structures is most compatible with such obstruction, either from BD lumen plugs or urinary tract obstruction from stones themselves.

Kidney International (2006) **69,** 2227–2235. doi:10.1038/sj.ki.5000268; published online 17 May 2006

KEYWORDS: kidney biopsy; kidney anatomy; renal injury; pathology; kidney stones

Correspondence: *AP Evan, Department of Anatomy and Cell Biology, Indiana University School of Medicine, 635 Barnhill Drive, MS 5055, Indianapolis, Indiana 46220, USA. E-mail: evan@anatomy.iupui.edu*

Received 4 November 2005; revised 6 December 2005; accepted 23 December 2005; published online 17 May 2006

Although Wollaston[1] first described 'cystic oxide' stone in 1810, we are aware of only one report detailing the renal histopathological changes in patients who have cystine stones.[2] The disease arises from genetic defects of dibasic amino-acid transporters that permit excessive cystine excretion.[3] The cystine crystallizes and forms stones.[4,5] Some renal injury must be presumed, as glomerular filtration rates, estimated from serum creatinine levels, is reduced.[6,7] Proteinuria not owing to thiol drugs has been mentioned.[2,6,8] Cystinuric patients are over-represented among stone formers (SF) who have lost a kidney.[9] High blood pressure has been mentioned as an association.[6]

Because cystine stones frequently are large, and are resistant to disruption via shock wave lithotripsy,[3,10] surgical treatments are common. Growth of stones and new stone formation can be rapid[11,12] and require multiple surgical treatments. One might imagine cystine crystals would form in the collecting ducts as water is extracted and pH reduced, plug tubules, perhaps injure collecting duct epithelial cells, and create a pathology based upon intra-renal obstruction.

Elsewhere, we have delineated the surgical anatomy, and gross and microscopic pathology of the renal papillae, medulla, and cortex of well-characterized stone patients.[13,14] Our most striking finding has been that histopathology and gross morphological abnormalities are specific to the type of stone disease present. Among calcium oxalate SF, we found only interstitial apatite deposits.[13] Among brushite (BR) SF, we found the same interstitial deposits accompanied by intra-luminal plugging of inner medullary collecting ducts (IMCD) and ducts of Bellini (BD) with apatite crystals.[14] Epithelial cell death and interstitial fibrosis was obvious in the medulla and cortex. Patients with stones owing to intestinal bypass procedures for obesity lacked interstitial deposits, but had intra-luminal apatite plugging, with interstitial fibrosis.[13] We present here our findings in seven patients with cystinuria. BD are plugged with deposits of cystine crystals, thin loops of Henle, and IMCD contain intra-luminal plugs of apatite crystals, and the medullary interstitium is fibrotic.

RESULTS

BD obstruction by crystals was observed at surgery

Papillary morphology varied over a wide range. At one extreme the papillae were normal (patient 1, Table 1 and Figure 1a). At the other extreme, papillae showed flattening and pallor, with enlarged BD (Figure 1d); between the extremes, we observed changes that included dilated BD and small regions of plaque (Figure 1b and c). Some dilated BD contained protruding plugs of crystalline material (Figure 1c). These plugs were not firmly attached to renal tissue. Some dilated BD contained no visible plugs. We observed small amounts of white plaque whose papillary percent surface coverage, with the exception of Case 5, was at the levels we have described among non-stone-forming people (Table 2).

In two patients, we documented stones that seemed at percutaneous nephrolithotomy (PNL) to lie under the urothelium. Upon unroofing the urothelial overlay during stone removal, the deposits were exposed and seemed to lie freely floating in a cavity (Figure 2a–d). The cavity seen in Figure 2c is continuous with a dilated BD (Figure 2b and c). We interpret this as release of a stone that plugged a BD, and created a cavitary dilation of the duct beneath the urothelium.

Papillary histopathology

Lumen crystals. As expected from the surgical findings, histopathology varied from normal (patient 1, Figure 3a, Table 1) to plugging, dilatation, and injury of IMCD (Figure 3b–d). Frequently, thin loops of Henle were plugged with crystals, a lesion we have encountered thus far (Figure 3c and d) only as a very rare event among BR SF. The thin limb and IMCD crystals were not birefringent by polarization microscopy, suggesting they might be apatite. The initial site of crystallization in thin limbs appears to be at the apical cell surface (Figure 4a). Of note, although we found thin loop of Henle basement membrane apatite plaque deposits, we never found such deposits in tubules that contained luminal apatite plugs.

In some BD, epithelial cells have migrated into the tubule lumen and surrounded masses of crystal (Figure 4b and c). These infolding BD cells appear to have altered their polarity, because the cells have attached themselves to the crystal mass via their basement membranes. By polarization microscopy, these BD crystal masses were highly birefringent (Figure 4c)

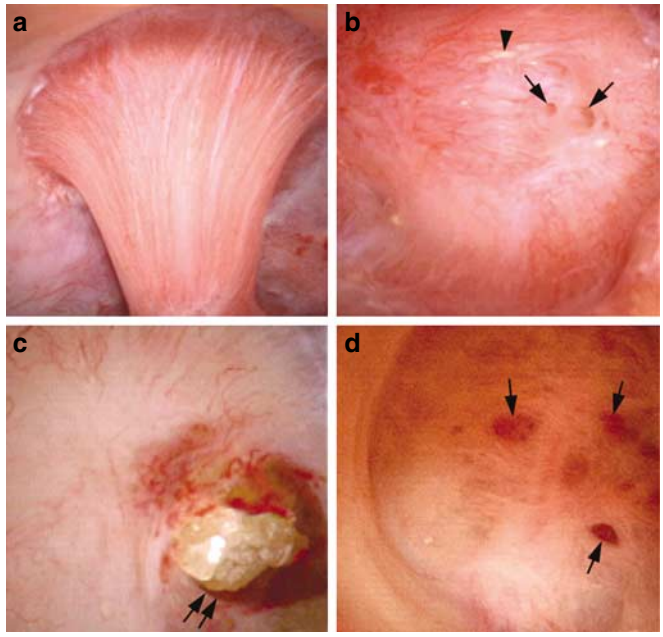

Figure 1 | Endoscopic views of papilla from cystine stone patients. Papillary morphology varies from (**a**) normal in patient 1 to (arrows) flattened with greatly enlarged openings of the (**b** and **d**) BD. (**c**) Some dilated BD contained protruding plugs of (double arrow) crystalline material. (**b**, arrowhead) Small sites of suburothelial white plaque , termed Randall's plaque, were noted.

Table 2 | Gross and microscopic changes of renal papillae

Case	Dilated bellini CD	Protruding stones	White plaque	Plaque area (%)	Loop CA Dep	Interst fibrosis	CD dilation
1	0/3	0/3	0/3	0.29	0	0	0
2	1/4	0/4	4/4	1.03	1	1	1
3	2/6	1/6	4/6	0.14	2	2	3
4	2/5	1/5	3/5	0.62	3	3	3
5	0/5	0/5	5/5	1.8	1	0	0
6	3/7	1/7	7/7	0.5	1	2	2
7L	5/9	3/9	5/9	0.6	1	1	1
7R	6/9	2/9	4/9	ND	1	3	2
All	19/48	8/48	32/48	—	—	—	—

Dilated bellini CD, collecting ducts; Protruding stones and white plaque refer to intra-operative observations of gross papillary architecture, no.; of papillae showing changes/no.; of papillae imaged; Loop Ca Dep, loop of Henle calcium deposits no.; loops involved); interstit fibrosis, interstitial fibrosis; CD dilation, microscopic CD dilatation without plugging. Loop calcium deposits, interstitial fibrosis, and CD dilatation are graded 0 (none), 1 (mild), 2 (moderate), and 3 (severe). Patient 7 had a PNL procedure carried out on the right (7R) and left (7L) kidney. Only the left kidney of this patient was mapped, so there is no determination (ND) for plaque area for the right kidney.

Table 1 | Clinical characteristics of biopsied cystine patients

Case	Sex	Age 1st stone (year)	Stones	ESWL	PNL	Procedures	UT infect	Age at Bx (year)
1	F	19	1	2/2	1/1	3/3	0	19
2	F	19	4	2/2	1/1	4/4	1	40
3	F	16	10	2/2	2/1	6/5	1+	64
4	F	18	15	3/3	4/4	8/8	1+	43
5	M	20	>100	>5/>5	1/1	>16/>16	0	31
6	F	45	2	0	1	1/1	0	47
7	F	27	25	0	5/1	5/1	0	52

ESWL, extracorporeal shock wave lithotripsy before Bx (Bx side); F, female; M, male; PNL, percutaneous nephrolithotomy before Bx (Bx side); Stones, number of stones before Bx; UT, urinary tract; procedures, total of all procedures (includes ESWL, PNL, ureteroscopy, open surgery, cystolithopaxy) before Bx (Bx side).

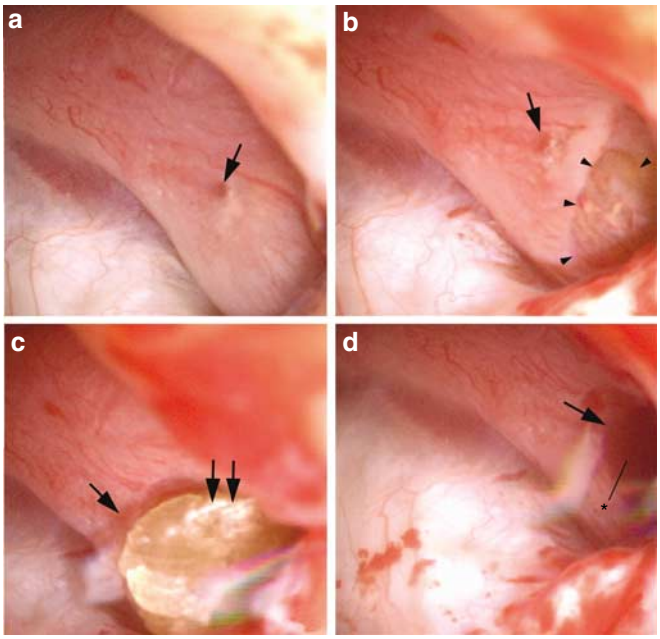

Figure 2 | Endoscopic unroofing of intra-luminal cystine deposits. (**a–d**, arrow) In two patients, large masses of crystalline material were seen at the time of PNL to lie under the urothelium at a site marked by a dilated BD. (**b**, arrowheads) Upon unroofing the urothelium during the biopsy procedure, (**c**, double arrow) deposits were exposed that were located within a tubular lumen. (**d**) Lumen of the (asterisk) BD after the deposit had been removed.

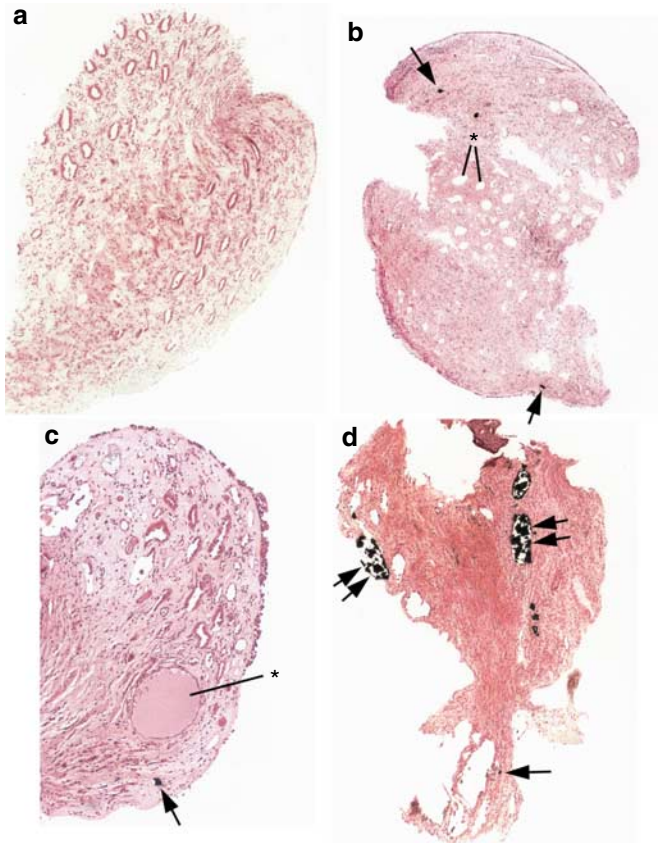

Figure 3 | Histological images of papillary biopsies from cystine stone formers. The papillary histopathology of the cystine patients varied from (**a**) normal to (**b–d**) regions of plugging, dilation, and injury of IMCD. Intra-luminal plugging with crystals was noted in (**b–d**, arrows) thin loops of Henle and (**d**, double arrows) IMCD. (**b** and **c**, asterisks) Dilated IMCDs without crystalline material were commonly seen. Original magnification, (**a**) × 700, (**b**) × 600,(**c**) × 800, and (**d**) × 550.

suggestive of cystine, but not apatite. Like thin loop crystal plugging, this lesion is also new in our observations of SF in that the crystal does not appear to be apatite.

Basement membrane crystals. Yasue staining for calcium deposits was positive at basement membranes of thin loops of Henle (Figure 5a–c) with extension into the interstitial space. This pattern is identical to the interstitial plaque found in calcium oxalate and BR SF, and has been called 'Randall's type 1 plaque. The amount of interstitial plaque is much less than what we have described[14] in calcium oxalate SF, and similar to what we found in non-stone-forming subjects.

Tissue changes. Papillary tissue was normal only in patients 1 and 5 (Table 1 and Figure 3a). All of the other patients showed focal sites of IMCD dilation with varying degrees of surrounding interstitial fibrosis (Figures 3b–d and 5b, c). In some regions (Figure 3b), IMCD dilation and fibrosis are mild. Other regions show marked dilation and interstitial fibrosis (Figures 3c, d, and 5c) as noted by loss of nephron segments and extensive interstitial scarring. In both loops of Henle and IMCD, epithelial cell injury varied from flattening to complete necrosis (Figure 6) exposing the basement membrane. An unusual amount of cellular debris was present in lumens of both thin loops and IMCD in areas of crystal-associated injury (Figure 6). We often noted dilated IMCD (Figure 3b and c) without lumen deposits but with cell flattening and occasional cast material. We could not identify an apparent cause of the dilation. By contrast, we never observed dilated BD without concomitant crystal plugging.

Relationship between surgical and histological findings

Table 2 makes clear that obstruction of BD, as assessed from intra-operative imaging of BD and protruding BD stones is associated with interstitial fibrosis as determined microscopically, almost 1:1. As well, dilation of IMCD is associated with BD dilatation (Table 2). These associations are important because one is made at surgery, whereas the others are from microscopy. Thin loop of Henle calcium deposits are also correlated with BD obstruction, although less convincingly. Some of the lowest values for creatinine clearance (Table 3) occur in the patients with the most marked BD obstruction. Overall, BD obstruction as seen grossly at surgery is a reasonable predictor of papillary histopathological changes.

Nature of crystal deposits

Cystine and apatite crystals were both identified, but in different nephron segments. The large plugs of crystals in BD

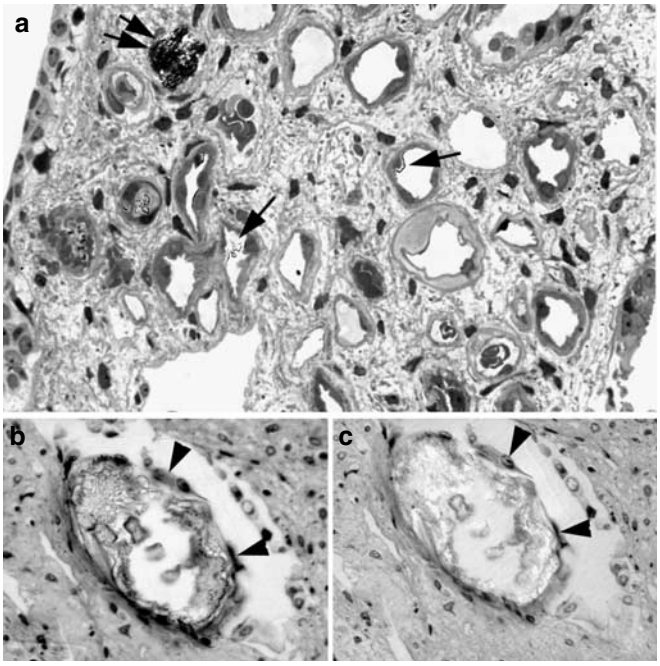

Figure 4 | Sites of crystalline deposition in loops of Henle and BD. (**a**, arrows) The initial site of crystallization in the thin loops of Henle appears to be at the apical cell surface. (**a**, double arrow) A site of complete plugging of the thin loop is seen. (**b** and **c**, arrowheads) Intra-luminal plugging also occurs in the BD where occasionally we observed layers of epithelial cells that are seen surrounding masses of crystals. Examination of crystalline material in the lumen of the BD (**b**) without and (**c**) with polarization microscopy suggests that the deposits are cystine and not apatite. Original magnification, (**a**) ×900, (**b**) ×1100, and (**c**) ×1100.

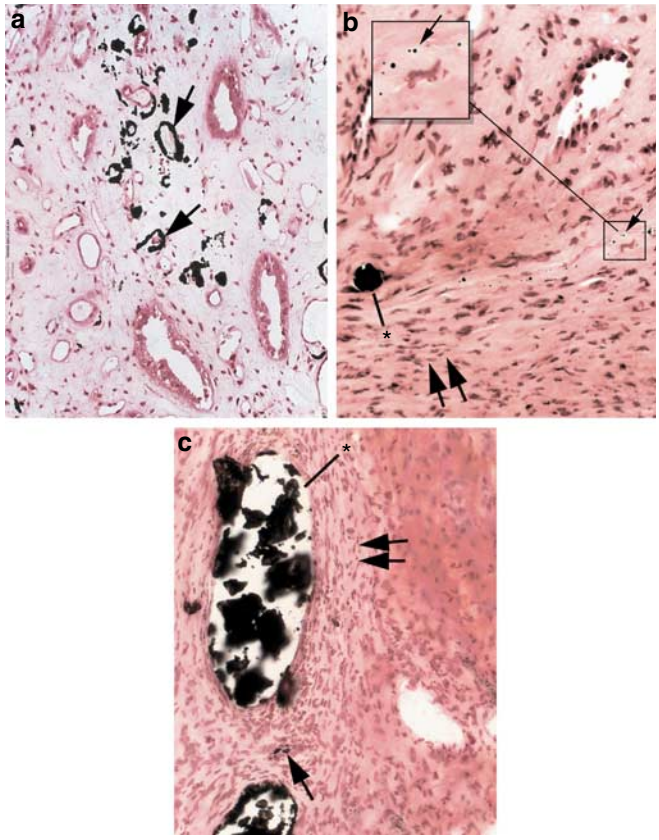

Figure 5 | Basement membrane and interstitial changes in cystine papillary biopsies. (**a**–**c**, arrows, magnified inset to **b**) Yasue staining for calcium detected tiny crystalline deposits in the basement membranes of thin loops of Henle, a pattern identical to the interstitial plaque termed Randall's type I plaque. (**b** and **c**, double arrows) Additional interstitial changes included varying degrees of interstitial fibrosis surrounding sites of intra-tubular crystalline deposits in either (**b**, asterisk) loops of Henle or (**c**, asterisk) IMCD. Original magnification, (**a**) ×900, (**b**) ×1200, and (**c**) and ×1100.

always were cystine (Figures 2c, 7, and 8). The large masses of intra-luminal crystals located in the BD could not be processed and cut with routine histological techniques. Therefore, biopsies with crystals protruding out of BD (Figure 7a) were imaged with a micro-CT (μCT) system to determine mineral composition of the crystalline deposits (Figure 7b–d). The large triangular area of mineral seen in Figure 7b had an attenuation value of 8500 indicating cystine. The IMCD and thin loop of Henle deposits (Figures 3c, d, 5b, and 7c d), however, were invariably apatite (Figures 8 and 9). In no deposits did we find cystine and apatite admixed.

Cortical changes

In the cortex, patient 1 showed no change. From patient 4 we do not have an adequate sample. For patients 2, 3, 5, 6, and 7 (left kidney), changes consisted of glomerular obsolescence, tubular atrophy, and interstitial fibrosis (Table 4, Figure 10a and b). The right kidney of patient 7, which had very severe papillary damage, showed severe glomerular obsolescence (Table 4).

We encountered an abnormality not hitherto observed among our stone-forming patients. In patients 3 and 7, we found Yasue-positive material in the basement membranes of the parietal epithelial layer of the glomeruli and distal convoluted tubule (Figure 10c and d). These deposits have the appearance of apatite plaque seen in the medulla. We could not perform infrared spectral analysis or transmission electron microscopy (TEM) owing to the sparseness of the deposits.

DISCUSSION

BD contain cystine

Perhaps more than any other of the stone-forming patients we have studied to date, cystinuria resembles BR stone disease in having BD and IMCD lumen plugging associated with interstitial fibrosis, glomerular atrophy, and cortical interstitial scarring.[14] One big difference is that the BD lumen plugs are composed exclusively of cystine, not apatite as in BR disease. They also differ in that cystine plugs are not fixed to renal tissue and are easily dislodged, whereas apatite BD plugs in BR SF are fixed and cannot be easily dislodged. That cystine might crystallize in BD lumens, plug them, and cause cell injury is not surprising in that water extraction is virtually complete and cystine concentrations would resemble

those in urine, which are high enough to cause crystallization and stones.

Obstruction of the BD and IMCD is associated with papillary interstitial fibrosis and with histologically evident IMCD dilation. We suggest, although we cannot prove, that BD obstruction with cystine is the primary driver of renal injury in cystinuria and leads to secondary IMCD dilation, as well as cortical interstitial fibrosis and moderate to severe glomerular injury. The presence of clinically significant albuminuria, by dipstick, in all but two of our patients may well reflect nephron injury. Such proteinuria has been recognized before.[2,6,8] In addition, Assimos *et al.*[7] have documented reduced renal function in cystinuria as did Dahlberg *et al.*[6] findings consistent with the pathology we describe. In a rat model of intestinal hyperoxaluria with IMCD plugging, we[15] also found extensive IMCD dilatation

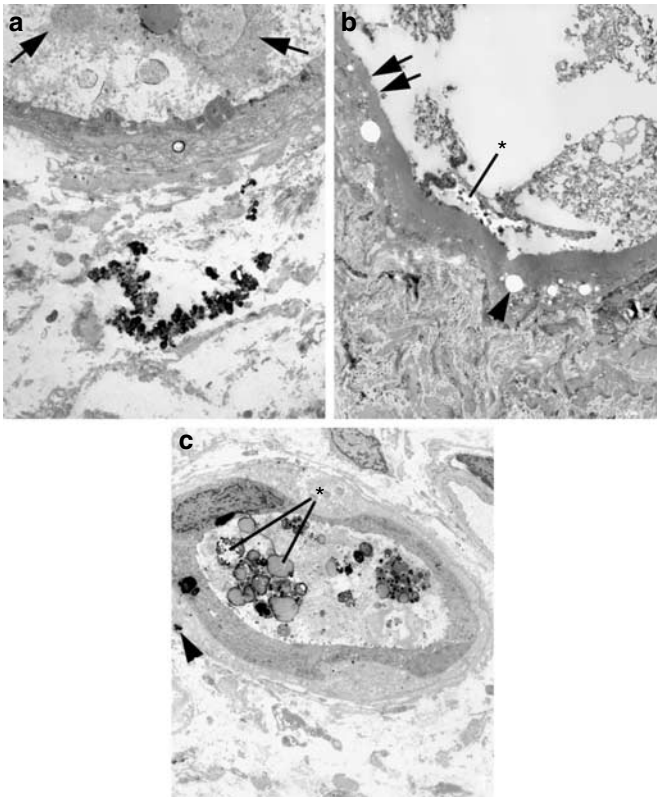

Figure 6 | Transmission electron microscopic images of cellular injury to thin loops of Henle. Epithelial cell injury ranged from an unusual amount of cellular debris in the (**a**, arrows) tubular lumen to frank necrosis exposing the (**b**, double arrow) tubular basement membrane. (**b** and **c**, asterisks) Crystalline material was seen admixed with cellular debris within the tubular lumen. Note the presence of crystalline deposits within the (**a**–**c**, arrowheads) basement membranes and in the interstitial space. Original magnification, (**a**) $\times$ 5000, (**b**) $\times$ 6000, and (**c**) $\times$ 5500.

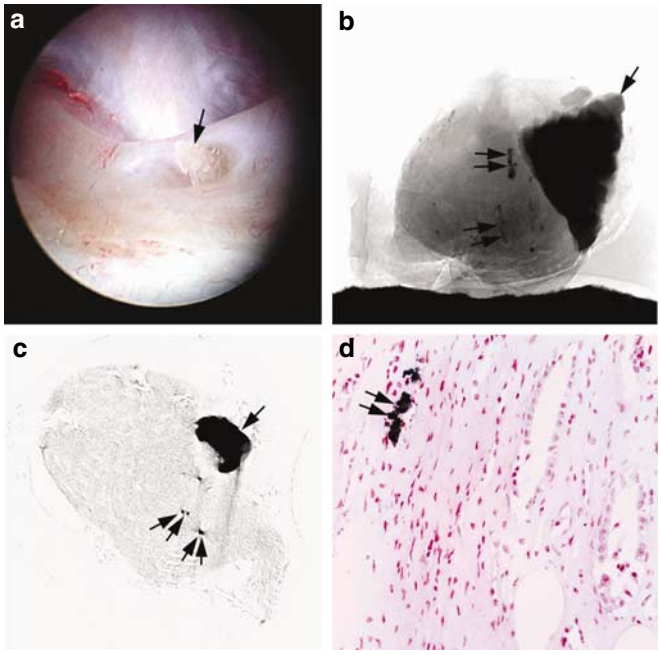

Figure 7 | Endoscopic and μCT images of papillary tissue with enlarged BD. (**a**) An endoscopic view of a papilla with an enlarged opening of a BD with a protruding plug of crystalline deposit (arrow). A papillary biopsy was obtained that included the dilated BD. (**b**) A three-dimensional reconstructed μCT image of that papillary biopsy and the arrow indicates the site of the protruding plug seen in (**a**). The large, dense triangular deposit was determined to have an attenuation value of 8500, a value consistent with cystine. Surrounding this large deposit are several smaller regions of (double arrow) mineral that all had an attenuation value of 22 000, a value consistent with apatite. A single μCT slice of the biopsy is seen in (**c**) where a portion of the (arrow) large and (double arrows) small deposits are clearly seen. This biopsy was divided in half. The upper half containing the large crystalline deposit was used for μ-Fourier transform infrared microspectroscopy analysis, whereas the lower half was embedded in paraffin for histopathogy. (**d**) A paraffin section from the lower half of the biopsy showing Yasue-positive material in a (double arrow) thin loop of Henle. Original magnification, (**d**) $\times$ 900.

Table 3 | Selected lababoratory values

Case	SCR	CCR	UCyst	ALB	Cyst SS	UpH	UVOL	UCA	UCIT	SS CAP
1	0.9	112	639	2+	1.03	6.79	0.95	127	669	2.14
2	1.3	67	NA	1+	NA	7.12	0.64	68	281	3.12
3	1.1	51	688	3+	0.95	6.88	2.55	43	363	0.2
4	1.0	77	621	2+	1.09	6.86	1.46	154	698	2.08
5	1.5	110	897	NEG	1.11	6.10	2.67	100	431	0.42
6	0.8	142	1031	3+	0.92	5.70	2.75	96	1300	0.16
7	1.7	49	486	NEG	1.08	7.00	0.75	48	522	1.38

ALB, urine albumin determined by clinical dipstick; CCR, creatinine clearance (ml/min); cyst SS, urine cystine supersaturation (Materials and Methods); NA, a urine sample was not available for this determination; SCR, serum creatinine (mg/dl); SS CAP, supersaturation with respect to calcium phosphate; UCA, calcium excretion (mg/24 h); UCIT citrate excretion (mg/24 h); UCyst, urine cystine (mg/day); UpH, pH of the 24 h urine sample; UVOL, urine volume (l/24 h).

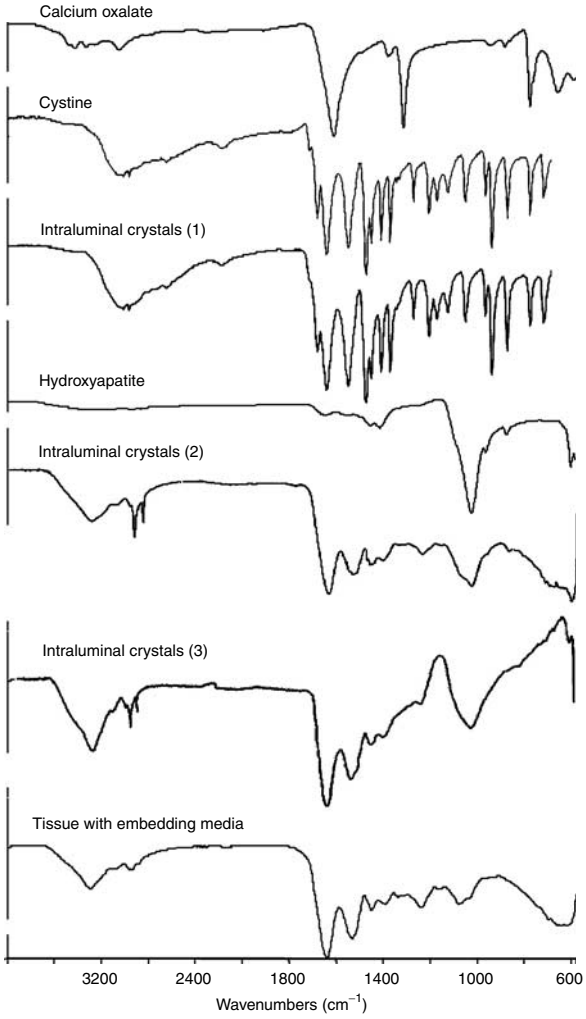

Figure 8 | μ-Fourier transform infrared microspectroscopy spectra of crystal deposits in cystine stone former. This figure illustrates a series of infrared spectra obtained for a set of standards (calcium oxalate, cystine, and hydroxyapatite). The spectrum for intra-luminal crystals (1), obtained from a region of deposit collected from the upper half of the biopsy seen in Figure 7, matched that of cystine. The spectrum obtained from intra-luminal crystals (2) in the thin limb of Henle's loop matched that of apatite, whereas intra-luminal crystals (2) was from a inner medullary collecting also matched with apatite.

above the plugs and in areas that themselves had no evidence for plugging. Obstruction within the renal pelvis is known[16] to cause dilated medullary collecting duct lumens, and patients 2–7 have had repeated stone passage and obstructive episodes, whereas patient 1 who has had only one stone has no IMCD dilatation.

The plugs of crystal protruding from BD lumens (Figures 1c and 7a) are entirely composed of cystine, but during surgery we found that they are loose and easily dislodged rather than firmly anchored within the BD lumen. This is consistent with the fact that none of the patients exhibited stones attached to the renal papillae. Given our findings, we suspect that plugs form and are spontaneously extruded. Extruded plugs could be the nidus for cystine stones in the renal pelvis. We find unattached stones frequently. The exact

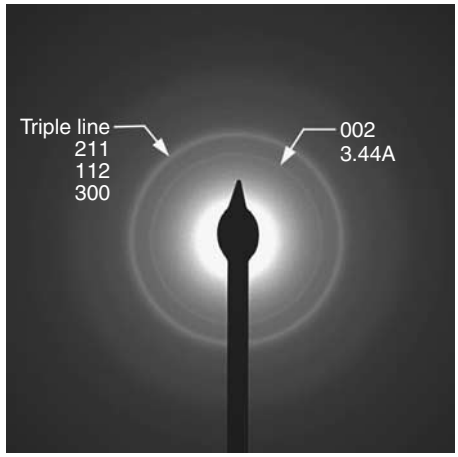

Figure 9 | TEM electron diffraction pattern of intra-luminal deposit in a cystine stone former. An area of intra-tubular crystal deposition (thin loop of Henle) from Case 3 was analyzed by electron diffraction and identified as biologic hydroxyapatite. The pattern shows the sharp 002 diffraction peak reflection, the elongated nature of the crystals, and the broad diffraction band containing the 211, 112, and 300 diffraction peaks, which is a characteristic of biologic apatite.

relationship between extruded plugs, stones growing on anchored plugs, and *de novo* cystine crystallization in the bulk phase pelvic urine-forming stones remains an open research issue.

Loops of Henle and IMCD contain apatite

No stone disease has ever been associated, thus far, with such extensive apatite deposits in the lumens of the thin loops as we describe here. All but one of our patients has this lesion. Rodent data reveal that thin loop fluid is normally supersaturated with respect to calcium phosphate phases, and fluids modeled *in vitro* to approximate thin limb fluid spontaneously produce a poorly crystalline apatite,[17] but *in vivo* manifestation of such crystallization has never before been found. Bostrum *et al.*[2] identified intra-tubular calcium phosphate-containing deposits in nine of 19 cases of cystinuria, but he localized them to the distal portion of the collecting ducts not the thin limbs. His samples were from nephrectomy and autopsy, not taken at surgery, and therefore are not strictly comparable to ours. We cannot account for the thin limb deposits, and consider them novel and a potential starting place for new research.

Of interest, thin loops plugged with apatite specifically do not show basement membrane apatite deposits. Such deposits are the apparent origin of Randall's plaque,[13] and these patients do possess normal amounts of plaque, but curiously we find basement membrane deposits only in otherwise normal thin loops. This bears upon the basic physiology of plaque development. One mechanism for plaque could be high supersaturation of thin limb fluid. That thin limbs plugged with apatite, surely produced by high lumen calcium phosphate supersaturation, have no basement membrane plaque is a point against loop fluid as a driver of plaque in basement membrane.

Table 4 | Cortical pathology of cystine stone formers

Stone group	Glomeruli	Glomerular pathology			Tubular atrophy	Interstitial fibrosis
		Mild	Moderate	Global		
CAOX (15)	152	10/5	11/2	0	1.2/10	1.2/10
BR (9)	193	3/1	41/6	68/2	1.8/9	2.3/9
Control (4)	264	2/2	0	0	0	0
Bypass (3)	38	2/2	9/1	0	1.5/2	1.5/2
Cystine (7)						
1	13	1	2	0	1	1
2	42	7	1	4	3	3
3	19	14	1	0	1	1
4	—	—	—	—	—	—
5	7	1	0	0	1	1
6	12	1	0	0	1	1
7L	28	2	0	0	1	1
7R	39	0	6	11	2	1

brushite, BR stone formers; bypass, patients with stones owing to intestinal bypass for obesity; CAOX, calcium oxalate stone formers; CaOx, BR, control and bypass are from a previous report;[13] control, control subjects; glomeruli, total number of glomeruli in group; glomerular pathology, findings about glomeruli, reported as number of glomeruli showing mild moderate or global changes (Materials and Methods); blank indicates no glomeruli show the changes for that column; tubular atrophy and interstitial fibrosis are graded in a scale of 0–3 intensity units as noted. Cystine patient 7 had a PNL procedure carried out on the right (7R) and left (7L) kidney. Note that cortical tissue was not obtained for cystine patient number 4.

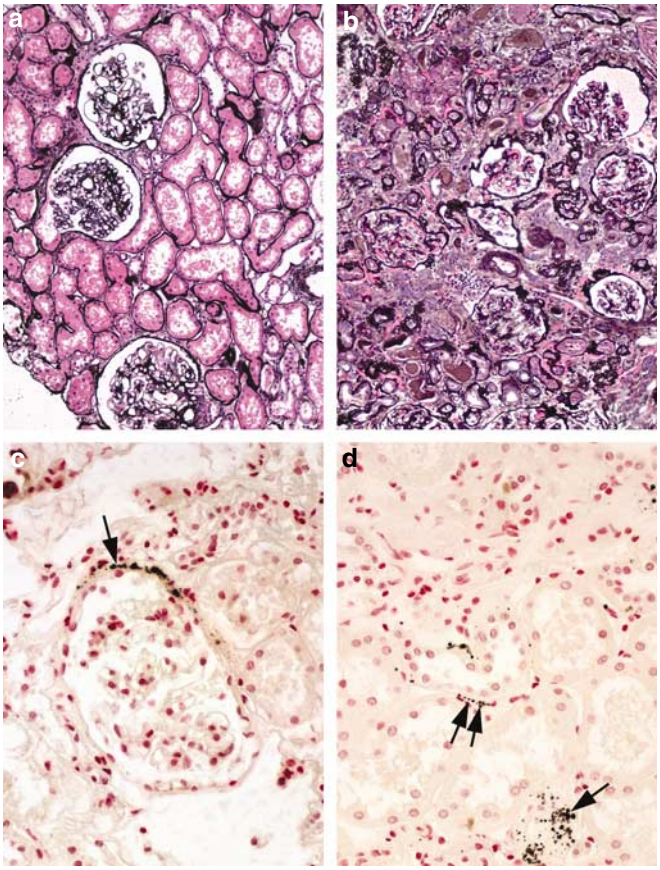

Figure 10 | Histopathology of cortical biopsies from cystine stone formers. Cortical biopsies from the cystine SF showed no changes (**a**) in patient 1 to a (**b**) moderate degree of glomerular obsolescence, tubular atrophy, and interstitial fibrosis . In addition, we observed Yasue-positive deposits in the basement membranes of the (**c** and **d**, arrows) parietal epithelial cells and (**d**, double arrows) distal convoluted tubules. Original magnification, (**a**) ×700, (**b**) ×700, (**c**) ×1100, and (**d**) ×1100.

IMCD apatite plugs were found in our BR SF and SF with intestinal bypass for obesity.[13,14] We do not have a physiological mechanism for their formation and consider this an open research issue. We have suggested that cell injury reduces acidification within individual nephron segments and permits apatite crystallization. Such a mechanism is compatible with the notably high urine pH values in our patients (Table 3) and reported in other patient series.[18] The high pH values reported here and previously were obtained in the absence of alkali treatment. Finally, one could mention but cannot document presently that alkali treatment for cystinuria could in principle increase thin loop and IMCD tubule fluid pH and foster apatite deposits. Such treatment is widely used in stone disease, yet apatite deposits appear confined to highly specific patient subgroups.

Stones can contain cystine and apatite

Although we never found apatite and cystine together in any renal deposits, mixing of calcium phosphates with cystine is well known in kidney stones. Among 248 cystine stones studied crystallographically, 81 were reported as admixed.[19–21] In a subset of 95 cystine stones for which more detail was given, 25 were reported to be admixed with as much as 25% apatite.[19,20] Given a very high frequency of urinary tract infection in patients with cystinuria,[6] struvite cannot be excluded. Idiopathic hypercalciuria may also be present in patients with cystinuria, as was the case in one of our seven, and foster calcium stones. A number of non-cystine stones have been reported as passed by patients with cystinuria, these are generally calcium stones.[2,6,8,18] Even so, BD lumens did not contain apatite crystals, so we must presume, for the moment, that apatite crystallizes upon cystine stones in the urinary tract, not within the BD lumen, and the admixture reflects events downstream from those in the BD itself.

Glomerular and distal convoluted tubule deposits

The tiny basement membrane deposits of Yasue-positive material at these sites have no apparent explanation. We have not observed such deposits in renal tissue from any other type of stone former studied to date. They have not *hitherto* been described in any human pathology.

Summary

Overall, cystine crystallizes in BD lumens with the probable result of upstream cell injury and interstitial reaction, nephron obstruction, glomerular loss, and cortical fibrosis. Thin loop lumens can show plugging with apatite crystals, a novel lesion not *hitherto* observed in such abundance and one we cannot presently explain. Because the lumens of BD contain the final urine, contemporary treatment approaches with hydration, increased pH, and thiol medications to prevent cystine stones could possibly ameliorate or – if begun early enough in life – prevent the BD lesions as well.

MATERIALS AND METHODS

Subjects

We studied all seven cystine SFs who required PNL at this institution (International Kidney Stone Institute, Methodist Clarian Hospital, Indianapolis, IN, USA) during the past 4 years (Table 1) and who consented to participate in the study. Patients were not selected. Clinical history was obtained along with reviews of old records to obtain stone analysis and type and number of stone procedures (Table 1). All seven formed pure cystine stones. Renal function as judged from serum creatinine levels and creatinine clearances were generally low (Table 3). Case 4 had two PNL procedures with biopsy, but detailed papillary imaging was carried out only on the right side. Case 7 had bilateral simultaneous PNL; mapping was performed on only the left side.

Clinical laboratory studies

Two 24 h urine samples were collected while patients were eating their free choice diet and off medications. In urine, we measured volume, pH, calcium, oxalate, citrate, phosphate, uric acid, sodium, potassium, magnesium, sulfate, and ammonia, and calculated supersaturation with respect to calcium oxalate, BR, and uric acid using methods detailed elsewhere.[22] In addition, for all but patient 2 (Table 3) we measured total cystine concentration,[23] and incubated an aliquot of each urine with an excess of solid-phase cystine crystals at 37°C for 96 h with stirring. At the end of the incubation, we measured the cystine concentration of the aliquot that represented the empirical solubility at that temperature. Supersaturation was calculated as the ratio of the initial to the post-incubation urine cystine concentration.[23] Routine clinical blood measurements were made on bloods drawn for clinical purposes.

Biopsy protocol

During PNL, all papillae were digitally imaged as described elsewhere.[24] Biopsies were taken from one upper pole, inter-polar, and lower pole papillum, and from the cortex except that only a cortical biopsy was obtained from the right kidney of patient 7. No biopsy site inspected intra-operatively displayed significant hemorrhage and no postoperative complications related to the biopsy procedures occurred in any patient. The study was approved by the Institutional Review Board Committee for Clarian Health Partners (No. 98-073).

Gross papillary morphology

Using digital video footage recorded during PNL, total surface area of each papilla was determined as described elsewhere[24] as was the surface area of interstitial deposits, which manifests as white 'plaque'. To do this, one of us (JL), without knowledge of the particular patient, outlined the areas of the entire papilla and the white plaque. The white plaque and total papillary areas were converted to pixels, giving percent papillary coverage with plaque. We recorded papillary morphology, scarring, and BD dilatation.[13,14]

Tissue analysis

General. Twenty-one papillary and eight cortical biopsies were studied using light electron microscopy and TEM. All biopsy (cortical and papillary) specimens from our first two cystine patients were immersed in 5% paraformaldehyde in 0.1 mol/l phosphate buffer (PPB) (pH 7.4). In the remaining five cystine patients, one cortical and two-thirds of the papillary biopsies were fixed in 100% ethanol to preserve the cystine crystals, whereas the remaining one-third of the papillary samples were immersed in PPB for ultrastructural analysis.

Light microscopy. Papillary and cortical biopsies fixed in PPB were dehydrated through a series of graded ethanol concentrations to 100% ethanol before embedment in a 50/50 mixture of Paraplast Xtra (Fisher Scientific, Itasca, IL, USA) and Peel-away Micro-Cut (Polysciences Inc., Warrington, PA, USA). Papillary biopsies fixed in 100% ethanol were directly embedded in a 50/50 mixture of Paraplast Xtra (Fisher) and Peel-away Micro-Cut (Polysciences). Twelve serial sections were cut at 4 μm and stained with the Yasue metal substitution method for calcium histochemistry,[25] hematoxylin and eosin for routine histological examination, or Jones' silver stain for the semiquantitation of glomerulosclerosis. An additional set of serial sections was cut at 7 μm for infrared analysis.

In a double-blind design, a renal pathologist (CLP) performed a semiquantitative analysis[14] using the Jones' silver-stained cortical sections from six of the seven cystine patients. Tubular atrophy and interstitial fibrosis were independently scored on a scale of 0–3 (0 = none, 1 = mild or $<34\%$ of sample, 2 = moderate or 34–66%, and 3 = severe or $>66\%$). Glomerulosclerosis was defined as increased mesangial matrix with or without wrinkling, thickening, and/or collapse of glomerular basement membranes. Sclerosis of individual glomeruli was scored as segmental ($<25\%$ = mild; 25–75% = moderate) or global ($>75\%$ = severe or total obsolescence). The total number of glomeruli observed and the number of glomeruli in each of the three categories of sclerosis were recorded.

Infrared. Attenuated total internal reflection Fourier transform infrared microspectroscopy was used as described elsewhere.[13]

Transmission electron microscopy. The 5-mm PPB and ethanol-fixed biopsy specimens of the renal papilla were divided into 1-mm blocks and routinely processed for TEM before embedment. Those tissue blocks processed for TEM that were fixed in PPB were first rinsed in phosphate buffer, and then dehydrated through a series of graded ethanol concentrations to 100% ethanol, passed through two changes of propylene oxide before embedment in Epon 812 (Electron Microscopy Science, Ft Washington, PA, USA). Those tissue blocks fixed in ETOH were rinsed in 100% ethanol and immediately passed through two changes of propylene oxide before embedment

in Epon 812. Thick sections ($\sim 1\,\mu$m) were stained with toluidine blue whereas the thin sections ($\sim 0.04\,\mu$m) were stained with uranyl acetate and lead citrate. All thin sections were examined with an FEI G2 Tecnai 12 BioTwin transmission electron microscope (FEI, Hillsboro, OR, USA), equipped with an AMT Corp., XR-60 Digital CCD system.

Electron diffraction. The structure of the crystalline material in ethanol-fixed papillary biopsies from one cystine patient was determined by TEM electron diffraction. The analysis was performed with a Philips Tecnai 20 at 100 kV and with a diffraction camera length of 890 mm. This sample had been routinely fixed for TEM but not stained.

μCT. All papillary biopsies underwent μCT analysis with the SkyScan-1072 (Vluchtenburgstraat 3, B-2630 Aartselaar, Belgium) high-resolution desk-top μCT system allowing non-destructive mapping of the location and size of the crystalline deposits within a biopsy specimen. This μCT system can generate a tissue window so that both the mineral deposit and tissue organization are seen at the same time. For this protocol, biopsies are quickly dipped in a 1:10 dilution of Hypaque (50%, Nycomed Inc., Princeton, NJ, USA)/phosphate-buffered saline, then coated with a thin layer of paraffin, and mounted in the center of a small chuck, which is then locked into place in the machine. The sample was positioned in the center of the beam, and the system configuration was set at 35 kV, 209 μA, 180° rotation, with flatfield correction. Images were saved to collecting ducts and reconstructed with Cone-Reconstruction software by SkyScan. These images were then reconstructed into three-dimensional images with SkyScan's CTAn + CTVol software. These images allowed us to orient properly each biopsy for future light microscopic analysis.

A second μCT system, the Scanco μCT 20 instrument (Scanco Medical AG, Basserdorf, Switzerland), was used to determine mineral composition of the crystalline deposits in three papillary biopsies analyzed by the SkyScan μCT device. This system does not generate a tissue window. We used our recently published method[26] to determine the μCT attenuation value for each crystalline deposit to determine its mineral composition. The attenuation value for cystine has a range between 8500 and 10 000, whereas apatite is 21 000–22 000. The system utilized a 7 μm spot-size microfocus X-ray source (0.16 mA, 50 kVp) that was detected by a charge-coupled device array with 1024 elements. The scans on each specimen were completed using standard resolution (512×512 pixels) and a 17.4 mm specimen holder, which produced image slice thicknesses and pixel widths of 34 μm.

ACKNOWLEDGMENTS

This work was supported by NIH Grant PO1 DK56788. We thank Dr James Williams and Molly Jackson for their help with the μCT analyses.

REFERENCES

1. Wollaston WH. On cystic oxide. A new species of urinaly calculus. *Trans R Soc Lond* 1810; **100**: 223–230.
2. Bostrom H, Hambraeus L. Cystinuria in Sweden. VII. Clinical, histo-pathological, and medico-social aspects of the disease. *Acta Med Scand* 1964; **411**(Suppl): 7–128.
3. Shekarriz B, Stoller ML. Cystinuria and other noncalcareous calculi. *Endocrinol Metab Clin N Am* 2002; **31**: 951–977.
4. Nakagawa Y, Asplin JR, Goldfarb DS *et al.* Clinical use of cystine supersaturation measurements. *J Urol* 2000; **164**: 1481–1485.
5. Pak CYC, Fuller CJ. Assessment of cystine solubility in urine and of heterogeneous nucleation. *J Urol* 1983; **129**: 1066–1070.
6. Dahlberg PJ, Van den Berg CJ, Kurtz SB *et al.* Clinical features and management of cystinuria. *Mayo Clin Proc* 1977; **52**: 533–542.
7. Assimos DG, Leslie SW, Ng C *et al.* The impact of cystinuria on renal function. *J Urol* 2002; **168**: 27–30.
8. Evans WP, Resnick MI, Boyce WH. Homozygous cystinuria – evaluation of 35 patients. *J Urol* 1982; **127**: 707–709.
9. Worcester E, Parks JH, Josephson MA *et al.* Causes and consequences of kidney loss in patients with nephrolithiasis. *Kidney Int* 2003; **64**: 2204–2213.
10. Dretler SP. Stone fragility – a new therapeutic distinction. *J Urol* 1988; **139**: 1124–1127.
11. Leusmann DB, Niggemann H, Roth S, von Ahlen H. Recurrence rates and severity of urinary calculi. *Scand J Urol Nephrol* 1995; **29**: 279–283.
12. Leusmann DB, Blaschke R, Schmandt W. Results of 5035 stone analyses: a contribution to epidemiology of urinary stone disease. *Scand J Urol Nephrol* 1990; **24**: 205–210.
13. Evan AP, Lingeman JE, Coe FL *et al.* Randall's plaque of patients with nephrolithiasis begins in basement membranes of thin loops of Henle. *J Clin Invest* 2003; **111**: 607–616.
14. Evan AP, Lingeman JE, Coe FL *et al.* Crystal-associated nephropathy in patients with brushite nephrolithiasis. *Kidney Int* 2005; **67**: 576–591.
15. O'Connor RC, Worcester EM, Evan AP *et al.* Nephrolithiasis and nephrocalcinosis in rats with small bowel resection. *Urol Res* 2005; **33**: 105–115.
16. Nagle RB, Bulger RE. Unilateral obstructive nephropathy in the rabbit. *Lab Invest* 1978; **38**: 270–278.
17. Asplin JR, Mandel NS, Coe FL. Evidence for calcium phosphate supersaturation in the loop of Henle. *Am J Phys* 1996; **270**: F604–F613.
18. Sakhaee K, Poindexter JR, Pak CYC. The spectrum of metabolic abnormalities in patients with cystine nephrolithiasis. *J Urol* 1989; **141**: 819–821.
19. Morriss RH, Beeler MF. X-ray diffraction analysis of 464 urinary calculi. *Am J Clin Pathol* 1967; **48**: 413–417.
20. Herring LC. Observations on the analysis of ten thousand urinary calculi. *J Urol* 1962; **88**: 545–562.
21. Daudon M, Donsimoni R, Hennequin C *et al.* Sex- and age-related composition of 10 617 calculi analyzed by infrared spectroscopy. *Urol Res* 1995; **23**: 319–326.
22. Parks JH, Worcester EM, Coe FL *et al.* Clinical implications of abundant calcium phosphate in routinely analyzed kidney stones. *Kidney Int* 2004; **66**: 777–785.
23. Nakagawa Y, Asplin JR, Goldfarb DS *et al.* Clinical use of cystine supersaturation measurements. *J Urol* 2000; **164**: 1481–1485.
24. Kuo RL, Lingeman JE, Evan AP *et al.* Urine calcium and volume predict coverage of renal papilla by Randall's plaque. *Kidney Int* 2003; **64**: 2150–2154.
25. Yasue T. Histochemical identification of calcium oxalate. *Acta Histochem Cytochem* 1969; **2**: 83–95.
26. Zarse CA, McAteer JA, Sommer AJ *et al.* Nondestructive stone analysis using μCT. *BMC Urol* 2004; **4**: 15–23.